IR permittivities for silicides and doped silicon

J. W. Cleary,[1] R. E. Peale,[1,*] D. J. Shelton,[2] G. D. Boreman,[2] C. W. Smith,[1] M. Ishigami,[1] R. Soref,[3] A. Drehman,[3] and W. R. Buchwald[3]

[1]*Department of Physics, University of Central Florida, Orlando, Florida 32816, USA*
[2]*College of Optics (CREOL), University of Central Florida, Orlando, Florida 32816, USA*
[3]*Sensors Directorate, Air Force Research Laboratory, Hanscom Air Force Base, Massachusetts 01731, USA*
**Corresponding author: peale@mail.ucf.edu*

Received October 2, 2009; revised January 26, 2010; accepted February 2, 2010;
posted February 16, 2010 (Doc. ID 118037); published March 23, 2010

The complex permittivity for Pt, Pd, Ni, and Ti-silicide films as well as heavily doped p- and n-type silicon were determined by ellipsometry over the energy range 0.031 eV to 4.0 eV. Fits to the Drude model gave bulk plasma and relaxation frequencies. Rutherford backscattering spectroscopy, X-ray diffraction, scanning electron microscopy, secondary ion mass spectrometry, and four-point probe measurements complemented the optical characterization. Calculations from measured permittivities of waveguide loss and mode confinement suggest that the considered materials are better suited for long-wavelength surface-plasmon-polariton waveguide applications than metal films. © 2010 Optical Society of America

OCIS codes: 240.6680, 250.5403, 160.3130, 160.3918, 260.3090, 120.4530.

1. INTRODUCTION

Bound electromagnetic waves that propagate along the interface between a dielectric and a conductor exist at frequencies below the plasma frequency of the conductor. These "surface plasmon polaritons" (SPP) are of interest for a variety of optical and optoelectronic applications [1–5]. In the long-wave IR (LWIR), SPP properties are adequately modeled using Drude theory, which casts the frequency-dependent permittivity in terms of a bulk plasma frequency ω_p and the electron relaxation frequency ω_τ. To sustain an SPP, the real part of the permittivity should be negative. Knowledge of material permittivity or, equivalently, the bulk plasma and relaxation frequencies, is essential when considering new materials for LWIR applications. The traditional SPP hosts are noble metals, but other materials such as silicides and doped semiconductors have been considered [6–8] at longer wavelengths. These nontraditional SPP hosts warrant consideration because of their inherent CMOS compatibility, which could benefit Si photonics and enable surface-plasmon-resonance (SPR) biosensors operating at vibrational-fingerprint wavelengths [9,10].

Optical constants of silicide films prepared by usual industrial processes have been previously investigated using ellipsometry in the visible (NiSi [11], $NiSi_2$ [11], Pd_2Si [12], PtSi [13,14], $TiSi_2$ [15]) and into the near-IR ($NiSi_2$ [16]). Reflectance measurements of thin films in conjunction with Kramers–Kronig analysis for $NiSi_2$ [17], PtSi [18], and $TiSi_2$ [19] have determined optical constants out to 124, 31, and 25 μm wavelength, respectively. Transmission and reflection have determined the optical constants of PtSi [20] out to 6 μm. Constants for single crystals of Pd_2Si [21] and $TiSi_2$ [22,23] have been determined by reflectance experiments and Kramers–Kronig analysis out to 25, 124, and 21 μm, respectively.

This work presents experimental determination of the permittivity values for Pt-, Pd-, Ni-, and Ti-silicides as well as n- and p-type doped silicon in the range 1–40 μm. Plasma and relaxation frequencies are extracted from fits to the Drude model, which allows extrapolation of the permittivity to 100 μm. All results are industrially relevant, since the materials were produced by standard processes used in the semiconductor device industry (CMOS processes). Benefits of using metal silicides or doped Si (as opposed to noble metals) in LWIR SPP waveguides are considered in terms of mode confinement and propagation loss.

2. EXPERIMENTAL

The silicide samples were prepared by first forming a native oxide on a ⟨100⟩ Si wafer via 10 min. insertion into a UV–ozone environment. This oxide was subsequently stripped with a hydrofluoric acid dip, rinsed in de-ionized water, and blown dry with nitrogen. Electron beam evaporation was used to deposit a Si film, followed by e-beam evaporation of Pt, Pd, Ni, or Ti with the film thicknesses given in Table 1. An 800°C, two-hour, post-metallization anneal diffused the metal into the Si to form the desired silicide. The doped p- and n-type Si samples were commercially obtained and had vendor specified resistivities of 0.0018–0.0032 Ω-cm and <0.014 Ω-cm, respectively. Resistivity data for heavily doped p- and n-Si in [24] determined a hole concentration in the p–Si samples to be $3-6\times10^{19}$ cm^{-3}, while the electron concentration in the n–Si exceeded 2×10^{18} cm^{-3}. An optically thick Ag layer was deposited on a Si wafer in the same manner as the silicide films for comparison.

Silicide film thicknesses were determined using a standard step profilometer and a PHI adept dynamic secondary ion mass spectroscopy (SIMS) system. A General IONIX 1.7 MU Tandetron Rutherford backscattering spectroscopy (RBS) system, with RUMP (Rutherford universal manipulation program) was used to investigate

Table 1. Metal and Si Thicknesses Used to Obtain Silicides of this Study, Silicide Characterization Results, and Extracted Drude Theory Parameters

	Ni	Pd	Pt	Ti	n–Si	p–Si
Si/metal (nm)	183/121	85/120	132/120	171/100	—	—
Profilometer thickness (nm)	230	160	200	180	—	—
SIMS film thickness (nm)	240	160	220	230	—	—
RBS film thickness (nm)	260	220	260	295	—	—
RBS composition	$NiSi_{1.38}$	$Pd_{2.13}Si$	$PtSi_{1.13}$	$TiSi_{2.03}$	—	—
ω_p (eV)	3.84	3.63	3.69	3.20	0.036	0.140
ω_τ (eV)	0.075	0.049	0.080	0.030	0.037	0.070
ρ_{fit} ($\mu\Omega$-cm)	37.8	27.7	43.7	21.8	18k	2.4k
Four-point probe ρ ($\mu\Omega$-cm)	31	21	31	12	14k	1.8k

sample stoichiometry [25] as well as silicide film thickness. Four-point probe measurements determined sample resistivity. Complex permittivities were determined using a J. A. Woollam IR-VASE and V-VASE ellipsometers in the IR and visible wavelength regions, respectively. The raw ellipsometer output was used to calculate permittivity data based on standard Fresnel equations assuming an optically thick film [26]. Finally, film morphology was studied using a Tescan Vega SEM (Scanning Electron Microscopy) and a Phillips XRG 3100 X-ray generator.

3. THEORETICAL

In Drude theory, the real ϵ' and imaginary ϵ'' parts of the complex permittivity are [27]

$$\epsilon' = \epsilon_\infty \left[1 - \frac{{\omega_p}^2}{{\omega_\tau}^2(1 + \omega^2/{\omega_\tau}^2)} \right] \tag{1}$$

and

$$\epsilon'' = \frac{\epsilon_\infty {\omega_p}^2}{\omega_\tau \omega(1 + \omega^2/{\omega_\tau}^2)}, \tag{2}$$

where ϵ_∞ is the permittivity of the material at frequencies well above the bulk plasma frequency ω_p. The relaxation frequency is $\omega_\tau = 1/\tau$ where τ is the relaxation time. The curve fitting of Eqs. (1) and (2) to measured permittivity gives the parameters ω_p and ω_τ. For silicides, ϵ_∞ is taken as unity, since it is assumed that the carrier concentration is sufficiently high to screen the polarization of the lattice, as in metals. For doped Si, ϵ_∞ is taken to be 11.7. Only that part of the data that qualitatively followed the expected Drude shape was used in the fit (at low frequencies ϵ' approaches a constant and ϵ'' increases as $1/\omega$). The ϵ' data generally follow the Drude model to higher frequencies better than do the ϵ'' data.

To assess the usefulness of these materials for SPP applications, the energy loss in the direction of SPP propagation as well as the characteristic penetration of the SPP electric field into the dielectric (in this case air) and into the conducting film were determined. For simplicity, we examined the asymmetric dielectric/conductor structure, although in practice the symmetric conductor/dielectric/conductor and dielectric/conductor/dielectric SPP waveguides offer superior performance [28]. The results for symmetric SPP infrared waveguides are quantified in [28]. The energy decay length in the direction of propagation, L_z, is given by

$$L_z = \frac{1}{2\,\mathrm{Im}(k(\omega))}, \tag{3}$$

where the complex plasmon wave-vector, $k(\omega)$, is

$$k(\omega) = \frac{\omega}{c}\sqrt{\frac{\epsilon_d \epsilon_c}{\epsilon_d + \epsilon_c}}, \tag{4}$$

with c the light speed and ϵ_d, ϵ_c the complex permittivity of dielectric and conductor, respectively [29]. The 1/e penetration depth of the SPP electric field [29] into the dielectric L_d or the conductor L_c is given by

$$L_{d,c} = \left[\frac{\omega}{c}\,\mathrm{Re}\sqrt{\frac{-{\epsilon_{d,c}}^2}{\epsilon_d + \epsilon_c}} \right]^{-1}. \tag{5}$$

The resistivity may be calculated from the Drude parameters according to

$$\rho = \omega_\tau / [\epsilon_\infty\, \epsilon_o\, {\omega_p}^2], \tag{6}$$

which may be compared with four-point probe measurements.

4. RESULTS

Scanning electron microscopy on the metal silicide films characterizes the film morphology. The nickel silicide SEM image is a mosaic of dark and light patches of ~ 2 μm scale in roughly equal proportions. Palladium and platinum silicide images appear to contain microcrystals with characteristic length scales of 2 and 1 μm, respectively. The titanium silicide film appears uniform and near-featureless, suggesting microcrystals of dimensions significantly smaller than 1 μm.

X-ray diffraction experiments were performed and results compared to powder diffraction standards (International Center for Diffraction Data, ICDD). All samples were measured using the Cu$K\alpha_1$ and Cu$K\alpha_2$ lines at wavelengths of 1.5406 Å and 1.5444 Å respectively, over an angular range of 20° to 80° with an angular resolution of 0.025°. All samples showed an intense peak identified as the (004) crystal plane of the bulk silicon substrate, as well as a weak (002) peak. The platinum-based film was

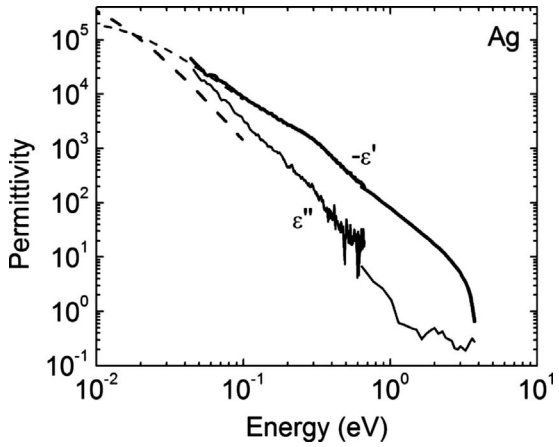

Fig. 1. Real and imaginary part of permittivity for Ag from ellipsometry data and data from [30]. Dashed curves show Drude fits.

well indexed (16 peaks) with polycrystalline platinum silicon (12.5 wt. % Si), but with a d-spacing 1–2% smaller according to the standard ICDD 7-251. The paladium-based film exhibited only the (400) and (800) planes of paladium silicide, indicating strong preferred orientation, and also a 3–6% smaller lattice spacing than the standard for Pd_2Si (ICDD 19-893). The titanium film was consistent with polycrystalline titanium silicide, with a lattice spacing matching the standard for $TiSi_2$ (ICDD 35-785). The nickel film was found to be consistent with the (211) and (013) crystal planes of nickel silicide, NiSi, (ICDD 38-844) although this film also shows a broad unidentified X-ray peak with a lattice spacing of 1.59 Å of unknown origin.

Thickness values of the silicide layers are summarized in Table 1. The full width at half-maximum (FWHM) of the metallic concentration versus depth from SIMS was taken as one measure of film thickness with ~10 nm uncertainty. The profilometer values agree within 10% except for titanium silicide. The thicknesses from RBS are systematically higher by more than the expected 5% uncertainty. The discrepancy may be due to surface oxide layers.

RBS results gave the metal-to-silicon ratios presented in Table 1. For Pd-, Pt-, and Ti-silicides, the ratios are nearly whole numbers. When taking into account the 5% uncertainty, the stochiometry of these silicides are nearest to Pd_2Si, PtSi, and $TiSi_2$. The nickel-to-silicon ratio deviated significantly from an integer.

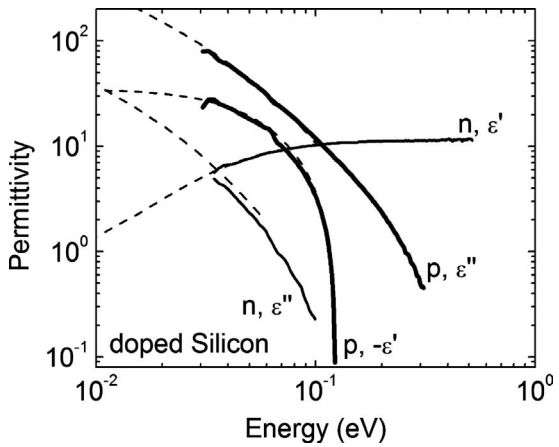

Fig. 2. Real and imaginary part of permittivity for doped Si from ellipsometry data. Dashed curves show Drude fits.

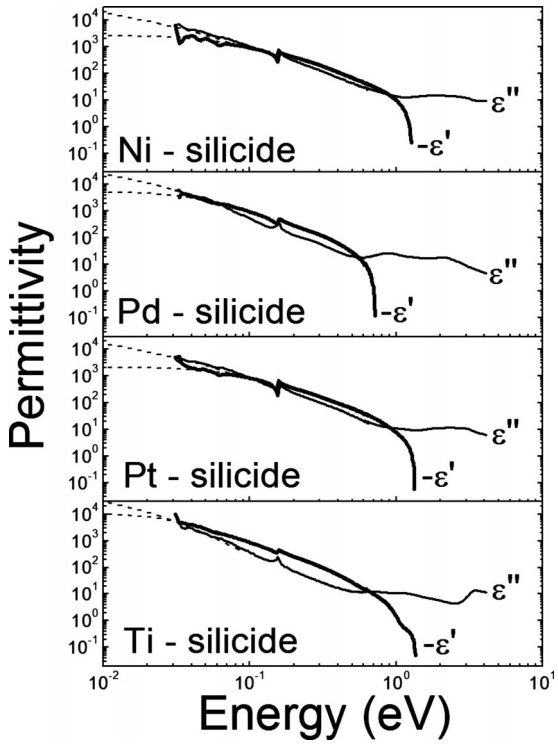

Fig. 3. Real and imaginary part of permittivity for metal silicides from ellipsometry data. Only negative values of real part are plotted in this figure. Dotted curves show Drude fits.

Figure 1 presents $-\epsilon'$ and ϵ'' spectra for Ag. Infra-red data measured for Ag was conjoined with visible data from [30]. Published ω_p and ω_τ values were used (9.02 and 0.018 eV, respectively [31]) to calculate Drude curves, which are plotted for wavelengths beyond 40 μm.

Figure 2 presents permittivity spectra for doped silicon. The ϵ' values for the n-Si sample were positive for all wavelengths investigated. Fitting emphasized the ϵ' data. Resulting ω_p and ω_τ values are given in Table 1. Extrapolation to wavelengths beyond 40 μm is plotted in Fig. 2.

Figure 3 presents permittivity spectra for metal silicides. Drude fits are also plotted (with ω_p and ω_τ values presented in Table 1). The curves for all silicides are similar at low photon energy. The upper limit for SPPs is significantly lower for Pd- than for the other silicides.

The ω_p and ω_τ values resulting from the fits to the IR data were used in Eq. (6) to calculate resistivity values, which are tabulated as ρ_{fit} and compared with four point probe values ρ in Table 1. The latter are systematically smaller than the ρ_{fit} values, as was also reported in [17] for various nickel silicides.

Figure 4 presents the characteristic plasmon propagation length as a function of free-space photon wavelength. Values calculated from permittivity data are plotted as symbols while the solid lines are extrapolations to longer wavelengths based on Drude theory and the extracted ω_p and ω_τ values. Only the range for which $\epsilon' < 0$ is plotted for each material. Because results for silicides are so similar, an average value of propagation length was plotted; the error bars represent the variation. For comparison,

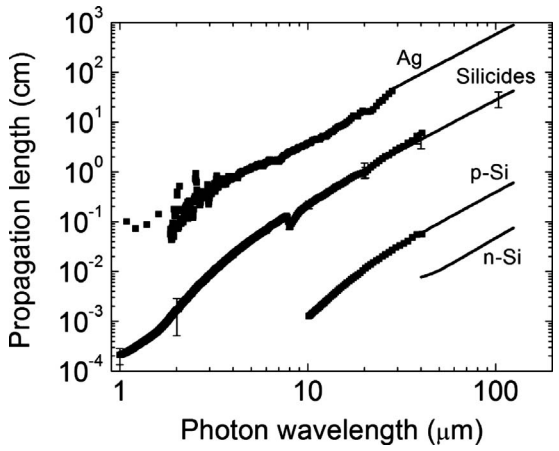

Fig. 4. Propagation length as a function of free-space wavelength. Symbols are calculated from experimental permittivity and curves are extrapolations based on Drude fits. The average of Pd, Ti, Ni, and Pt-silicides is plotted with error bars indicating the spread in their values. Results for Ag, included for comparison purposes, are calculated from experimental data (ours and [30]).

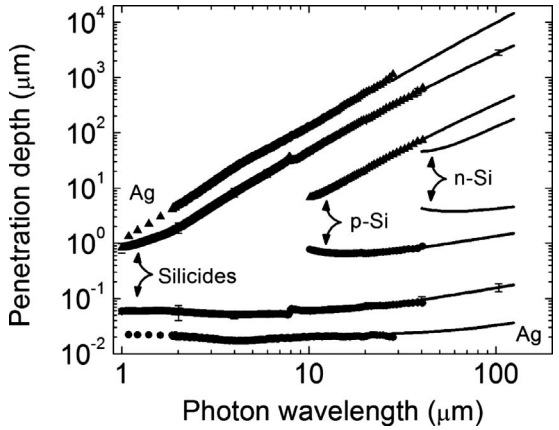

Fig. 5. Penetration depths versus free-space wavelength. Symbols are calculated from experimental permittivity and curves are extrapolations based on Drude fits. The average of Pd, Ti, Ni, and Pt-silicides is plotted with error bars indicating the spread in their values. Upper four curves (triangles) show penetration depth into air while the lower four curves (circles) show penetration depth into the conductor. Results for Ag, included for comparison purposes, are calculated from experimental data (ours and [30]).

near-IR propagation lengths based on measured permittivity are included for Ag [30]. No experimental values are presented for n-Si in Fig. 4 since $\epsilon' > 0$ for all experimental wavelengths, and the plotted curve is Drude extrapolation.

Figure 5 presents SPP field penetration depth into the conductor L_c (lower curves) and into air L_d (upper curves) as functions of free-space wavelength, according to Eq. (5). All symbols and curves in Fig. 5 are as in Fig. 4. For Ag, the field penetration depth into air everywhere exceeds the free-space wavelength. For silicides, the penetration depth into air is less than the wavelength for $\lambda < 2\ \mu$m. For the p-Si and n-Si, the penetration depth is less than the wavelength for $\lambda < 20\ \mu$m and 50 μm, respectively.

5. DISCUSSION

The RBS data suggest that the nickel silicide film is a mixture of NiSi and $NiSi_2$, while XRD indicates NiSi plus some unknown material. This may explain the mottled appearance in the SEM image if the forms exist in unmixed islands. Reference [11] reports the formation of $NiSi_2$ for annealing above 700°C and the formation of NiSi at 400°C. Our anneal of 800°C gave a nickel silicide that was most likely in the transition process from NiSi to $NiSi_2$ Our ω_p and ω_τ values of 3.84 and 0.075 eV, respectively, fall between those reported [17] for NiSi and $NiSi_2$ (see Table 2).

Table 2 presents published Drude parameters for the metal silicides. Our ω_p value in Table 1 for Pd_2Si agrees most closely with the reported value (3.6 eV) for polarization parallel to the single crystal c axis [21]. This result is in agreement with the observation from XRD that the Pd-silicide film consists of highly oriented microcrystals. The Pd_2Si relaxation frequencies differ by a factor of 1.6. The PtSi ω_p and ω_τ values in Tables 1 and 2 are in good agreement. For $TiSi_2$, ω_p differs by 30% while ω_τ differs by a factor of 2.

Table 2 lists published resistivity values for silicides, ρ_{pub}. Our ρ value for the nickel silicide sample falls into the reported range for NiSi, but it is below the range for $NiSi_2$. All ρ values for the other silicides fall within the respective ρ_{pub} ranges.

We have previously modeled [28] the impurity concentration dependence of ω_p and ω_τ in heavily doped Si. For both n-Si and p-Si, and we find that ω_p increases by a factor of 3.2 when n (or p) increases from 10^{20} cm^{-3} to 10^{21} cm^{-3}, whereas ω_τ remains essentially constant over that range.

Figures 4 and 5 suggest that silicides are more suitable for SPP applications at photon wavelengths in the range 5 to 100 μm [6] than are metal films due to better mode confinement while maintaining an acceptable propagation length. Doped Si is best suited for SPP applications at 50 to 200 μm wavelengths, i.e., the THz spectral range. These SPP hosts may also be exploited in LWIR surface plasmon resonance (SPR) biosensors, where characteristic vibrations should yield better specificity and sensitivity due to dispersion [9].

Table 2. Published Silicide Drude Parameters and Reported Resistivity Values

	NiSi	$NiSi_2$	Pd_2Si	PtSi	$TiSi_2$
ω_p (eV)	3.8 [17]	4.6–7.4 [16,17]	2.8–3.6 [21]	—	4.2 [22]
ω_τ (eV)	0.035 [17]	0.15–0.25 [16,17]	0.03 [21]	—	0.015 [22]
ρ_{pub} ($\mu\Omega$-cm)	12–36 [11,17]	34–60 [11,16,17,32]	13–35 [12,32,33]	28–35 [14,32]	10–25 [22,32,34,35]

ACKNOWLEDGMENTS

This work was supported by U.S. Air Force Office of Scientific Research (AFOSR) contract numbers FA8718-07C-0036, FA8718-06-C-0076, FA95501010030, and LRIR 09RY09COR (Gernot Pomrenke).

REFERENCES

1. M. L. Brongersma and P. G. Kik, *Surface Plasmon Nanophotonics* (Springer, 2007).
2. S. A. Maier, *Plasmonics: Fundamentals and Applications* (Springer, 2007).
3. R. R. Musin, Q. Xing, Y. Li, M. Hu, L. Chai, Q. Wang, Y. M. Mikhailova, M. M. Nazarov, A. P. Shkurinov, and A. M. Zheltikov, "Design rules for phase-matched terahertz surface electromagnetic wave generation by optical rectification in a nonlinear planar waveguide," Appl. Opt. **47**, 489–494 (2008).
4. C. Sirtori, J. Faist, F. Capasso, D. L. Sivco, A. L. Hutchinson, and A. Y. Cho, "Quantum cascade laser with plasmon-enhanced waveguide operating at 8.4 μm wavelength," Appl. Phys. Lett. **66**, 3242–3244 (1995).
5. A. Boltasseva, T. Nikolajsen, K. Leosson, K. Kjaer, M. S. Larsen, and S. I. Bozhevolnyi, "Integrated optical components utilizing long-range surface plasmon polaritons," J. Lightwave Technol. **23**, 413–422 (2005).
6. R. Soref, R. E. Peale, and W. Buchwald, "Longwave plasmonics on doped silicon and silicides," Opt. Express **16**, 6507–6514 (2008).
7. A. Sellai, P. G. Mc Cafferty, P. Dawson, S. H. Raza, and H. S. Gamble, "Surface plasmons on PtSi for visible and infrared Schottky barrier enhanced detection," Proc. SPIE **1735**, 240–249 (1992).
8. A. Sellai, P. Dawson, W. R. Hendren, S. H. S. Magill, and H. S. Gamble, "Infra-red surface plasmons on platinum silicide," Electron. Lett. **28**, 164–165 (1992).
9. J. Cleary, R. E. Peale, D. Shelton, G. Boreman, R. Soref, and W. Buchwald, "Silicides for infrared surface plasmon resonance biosensors," Mater. Res. Soc. Symp. Proc. 1133-AA10-03 (2008).
10. Y. Chen, "Development of mid-infrared surface plasmon resonance-based sensors with highly-doped silicon for biomedical and chemical applications," Opt. Express **17**, 3130–3140 (2009).
11. H. Chen and J. Lue, "Ellipsometry measurements of nickel silicides," J. Appl. Phys. **59**, 2165–2167 (1986).
12. J. H. Lue, H. Chen, and S. Lew, "Optical constants of palladium silicides measured by a multiple-wavelength ellipsometer," Phys. Rev. B **34**, 5438–5442 (1986).
13. H. Bentmann, A. Demkov, R. Gregory, and S. Zollner, "Electronic, optical and surface properties of PtSi thin film," Phys. Rev. B **78**, 205302 (2008).
14. J. Lue and S. Mu, "Ellipsometry and structural studies of chromium, molybdenum, and platinum silicides," Phys. Rev. B **36**, 1657–1661 (1987).
15. K. Lee and J. T. Lue, "Formation of titanium silicides and their refractive index measurements," Phys. Lett. A **125**, 271–275 (1987).
16. J. R. Jimenez, Z. Wu, L. J. Schowaiter, B. D. Hunt, R. W. Fathauer, P. J. Grunthaner, and T. L. Lin, "Optical properties of epitaxial $CoSi_2$ and $NiSi_2$ films on silicon," J. Appl. Phys. **66**, 2738–2741 (1989).
17. M. Amiotti, A. Borghesi, G. Guizzetti, and F. Nava, "Optical properties of polycrystalline nickel silicides," Phys. Rev. B **42**, 8939–8946 (1990).
18. J. M. Pimbley and W. Katz, "Infrared optical constants of PtSi," Appl. Phys. Lett. **42**, 984–986 (1983).
19. W. Henrion and H. Lange, "Optical properties of high-refractory disilicide thin films," Phys. Status Solidi B **151**, 375–382 (1989).
20. J. M. Mooney, "Infrared optical absorption of thin PtSi films between 1 and 6 μm," J. Appl. Phys. **64**, 4664–4667 (1988).
21. M. Amiotti, G. Guizzetti, F. Marabelli, A. Piaggi, V. N. Antonov, Vl. N. Antonov, O. Jepsen, O. K. Andersen, A. Borghesi, F. Nava, V. V. Nemonshkalendo, R. Madar, and A. Rouault, "Optical properties of Pd_2Si," Phys. Rev. B **45**, 13285–13292 (1992).
22. A. Borghesi, A. Piaggi, G. Guizzetti, F. Levy, M. Tanaka, and H. Fukutani, "Optical properties of single-crystal titanium disilicide," Phys. Rev. B **40**, 1611–1615 (1989).
23. M. Tanaka, S. Kurita, M. Fujisawa, and F. Levy, "Dielectric properties of single-crystal $TiSi_2$ from 0.6 to 20 eV," Phys. Rev. B **43**, 9133–9137 (1991).
24. S. M. Sze, *Physics of Semiconductor Devices* (John Wiley & Sons, 1981).
25. L. R. Doolittle, "A semiautomatic algorithm for Rutherford backscattering analysis," Nucl. Instrum. Methods Phys. Res. B **15**, 227–231 (1986).
26. H. G. Tompkins and E. A. Irene, *Handbook of Ellipsometry* (William Andrew, 2005).
27. P. Y. Yu and M. Cardona, *Fundamentals of Semiconductors* (Springer, 1996).
28. R. Soref, S.-Y. Cho, W. Buchwald, R. E. Peale, and J. Cleary, "Silicon plasmonic waveguides," Chapter 1 in *An Introduction to Silicon Photonics*, S. Fathpour and B. Jalali, eds. (Taylor and Francis, 2010).
29. H. Raether, *Surface Plasmons on Smooth and Rough Surfaces and on Gratings* (Springer, 1988).
30. P. B. Johnson, R. W. Christy, "Optical constants of the noble metals," Phys. Rev. B **6**, 4370–4379 (1972).
31. M. A. Ordal, R. J. Bell, R. W. Alexander, L. L. Long, and M. R. Querry, "Optical properties of fourteen metals in the infrared and far infrared: Al, Co, Cu, Au, Fe, Pb, Mo, Ni, Pd, Pt, Ag, Ti, V and W," Appl. Opt. **24**, 4493–4499 (1985).
32. S. P. Mararka, *Silicides for VSLI Applications* (Academic, 1983).
33. R. Marani, R. Nava, A. Rouault, R. Madar, and J. P. Senateur, "Crystal growth, charaterisation and resistivity measurements of Pd_2Si single crystals," J. Phys.: Condens. Matter **1**, 5887–5893 (1989).
34. K. K. Ng, *Complete Guide to Semiconductor Devices*, 2nd ed. (Wiley, 2002).
35. K. Maex and M. Van Rossum, *Properties of Metal Silicides* (Short Run Press, 1995).